INDIAN JOURNAL OF SCIENCE AND TECHNOLOGY

RESEARCH ARTICLE

A Discrete Wavelet Transform and Dense CNN for Hyperspectral Imaging-Based Bloodstain Classification

Tejaskumar B Sheth[1]*, **Milind S Shah**[2]

1 Research Scholar, Gujarat Technological University, Gandhinagar, Gujarat, India
2 Professor and HOD, EC Department, Shantilal Shah Engineering College, Bhavnagar, Gujarat, India

OPEN ACCESS

Received: 07-07-2023
Accepted: 30-09-2023
Published: 13-11-2023

Citation: Sheth TB, Shah MS (2023) A Discrete Wavelet Transform and Dense CNN for Hyperspectral Imaging-Based Bloodstain Classification. Indian Journal of Science and Technology 16(42): 3795-3802. https://doi.org/10.17485/IJST/v16i42.1682

* **Corresponding author**.

199999915522@gtu.edu.in

Funding: None

Competing Interests: None

Published By Indian Society for Education and Environment (iSee)

ISSN
Print: 0974-6846
Electronic: 0974-5645

Abstract

Objectives: To maximize the identification and improve the accuracy of classifying the bloodstain in a hyperspectral image (HSI) at the crime scene, a 3-D discrete wavelet transform (3-D DWT) Dense CNN deep learning model is proposed in this work. **Methods:** This work proposes the use of a 3-D DWT to pre-process HSI data to effectively extract both spatial and spectral information while maintaining robust feature representation capabilities. Then, 3-D CNN that integrates dense connections attaches great importance to the reuse of features for classification. The experiment was carried out with the initial training/testing ratio set to 10/90 of the data samples, and we compared the results with four different state-of-the-art CNN architectures. **Findings:** The experimental results show that the 3-D DWT Dense CNN deep learning model achieves 97% classification accuracy, smoother classification maps, and more discriminable features for hyperspectral image classification. **Novelty and Application:** This work provides a deep learning 3D dense CNN model with the 3-D DWT and achieves improved identification of bloodstains at a messy crime scene. The proposed model requires a smaller number of trainable parameters, less computational power, so it can be used in the field of forensic science, where substance classification at the scene is important.

Keywords: Hyperspectral Imaging; Blood Strain Classification; Discrete Wavelet Transform (DWT); 3D CNN; Dense Connection; Forensic Science

1 Introduction

Bloodstain identification is a crucial aspect of forensic investigation at a crime scene. A variety of techniques are available for this purpose, including chemical enhancement techniques and the use of light sources with 15-30 nm bandwidths, which increase the contrast between a trace and its background. Many of these techniques, however, are either destructive or subject to human interpretation. Although various chemical-based blood identification techniques produce excellent results, but they damage blood samples collected from crime scenes, rendering them unusable for DNA extraction or retesting[(1)].

To avoid contamination of sample over the time various non-contact, non-destructive techniques have been developed and used in the field of forensic science. Different spectroscopic techniques such as Raman, Reflectance, Electron Paramagnetic Resonance (EPR), Nuclear Magnetic Resonance (NMR), and Infrared (IR) spectroscopies such as Attenuated Total Reflectance Fourier Transform IR spectroscopy (ATR-FTIR) are used by practitioners. For bloodstain identification, IR and Raman-based techniques yield promising results [2]. All these spectroscopy techniques are used the spectral information of bloods and did not consider spatial information or image area under observation.

HSI is appropriate for non-contact identification of evidence, reducing the risk of contamination and trace destruction. HSI combines conventional imaging and spectroscopy to produce a three-dimensional data set containing both spatial and spectral information of a crime scene. HSI is like a stack of images, each acquired at a specific spectral band. HSI, like spectroscopy, is available in various range of the electromagnetic spectrum, such as ultraviolet (UV), visible (Vis), near infrared (NIR), mid infrared (IR), and even thermal infrared [3].

The HSI technique is an excellent technique that extracts from a specimen both spectral and spatial information, producing a three-dimensional data set. It combines spectroscopy technique with conventional imaging, obtaining hyperspectral images by measuring numerous narrow wavelength regions with high resolution.

Human blood has distinct spectral characteristics that can be identified in hyperspectral data. Haemoglobin is the main component in blood that absorbs and scatters light in a characteristic manner, resulting in distinct absorption features in the visible and near-infrared (NIR) regions of the electromagnetic spectrum. By examining the spectral reflectance of different pixels in the image across various wavelengths, it is possible to detect the presence of blood. Reflected spectra with resolutions as low as 10 nm can be treated as miniature spectrographs which can be used to detect very small droplet of blood on the crime senses [4].

The advantages of using HIS in-crime scene investigation include faster data acquisition, reduce need of trained laboratory technician, no specimen preparation, reduced human error, no trace destruction, no specimen preparation, and the ability to produce consistent visual results.

Recent studies in the field of HSI classification in remote sensing and other applications show that Deep Learning improves accuracy. HSI is primarily concerned with three-dimensional data, and DL models have exploited spectral, spatial, and both spectral-spatial features. Aside from kernel and dimension reduction methods, DL methods automatically extract features and solve non-linearity problems. Convolutional Neural Networks (CNNs), Long Short Term Memory Networks (LSTMs), Multilayer Perceptron (MLPs), Deep Belief Networks (DBNs), and other DL models are commonly used for HIS classification. In HIS classification CNN gives better accuracy among the various deep learning methods [5].

In [6], the paper presents a non-destructive method for bloodstain identification using HSI that can identify blood samples with aging up to 3 days. In the work stated PCA was used with SVM, KNN, AN, and RNN.

In [7], author compares the performance of different deep learning architectures 1D CNN, 2D CNN, 3D CNN, RNN with baseline results of Support Vector Machine (SVM) to identify the bloodstain. The various deep learning methods show 74-94% accuracy with training and testing sample of 75-25%.

In [8], the paper proposes the use of a fast and compact hybrid CNN to process HSI data for bloodstain ID classification. The experiment's results were compared with state-of-the-art 3D CNN models and show 90% accuracy with a restricted sample size of 5%.

The CNN models typically produce a large number of learnable parameters, so the training process needs a lot of samples with labels on them in order to ensure classification accuracy. There aren't many labelled samples available because collecting labelled samples for HSI is expensive. In recent years numbers of methods are proposed for HIS classification with limited labels training samples [9].

As a result, some models, like fast dense spectral-spatial convolution (FDSSC) [10] and multiple spectral resolution (MSR)-3-DCNN [11], included the residual or dense connection to obtain multi-level features.

The classification performance of HSI is improved by applying feature reduction techniques through feature extraction and feature selection approaches. Among the existing HSI feature extraction techniques, the three-dimension discrete wavelet transform (3-D DWT) transformation has received a lot of attention due to its improved ability to extract robust spatial-spectral features of various scales and orientations [12]. Integrating 3D DWT with dense CNN outperforms existing state-of-the-art HSI classification approaches [13].

Our study focused on the combining the advantage of 3-D DWT for spectral component as preprocessing and Dense CNN network for compactness and strong capacity of learning to improve HSI classification performance. In total, our approach reduces the network complexity, calls for fewer parameters, shortens training and testing times, and achieves high classification performance with little training data.

2 Methodology

In our study, we focused on the 3-D DWT, and a slim and compact CNN network structure. The use of 3-D DWT enhances the interpretation and scale analysis capabilities of followed Dense CNN model. As a result, the combined usage of CNN and 3-D DWT can produce features with improved resilience against changes in scale and orientation. The flowing subsection explain the implementation of 3-D DWT Dense CNN classification model.

Let's make a HSI cube, denoted as $X \in R\ H \times W \times B$. Where, H and W represent the height and width of the spatial dimensions, respectively, while B indicates the number of spectral bands. To represent different blood and blood-like substances, a one-hot label vector $Y = (y1, y2,..., yC) \in R1 \times 1 \times C$, is used, where C signifies the total number of categories.

2.1 General Overview of the Proposed Approach

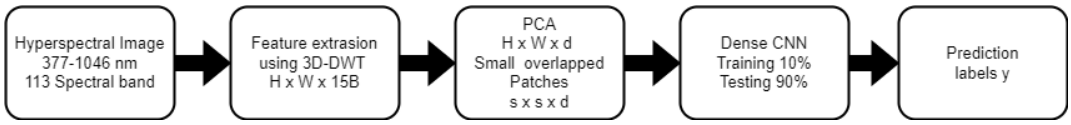

Fig 1. Overview of Implemented framework for HIS Classification

Figure 1 depicts the implemented framework for HSI classification. First, 3-D DWT is used as a preprocessing operation for HSI, which can extract spatial and spectral features simultaneously. In the spectral dimension, the principal component analysis (PCA) algorithm is used to reduce dimensionality and extract the most informative components. Because 3-D CNN requires both spectral and spatial information, the HSI cube is cropped into small, overlapped patches as samples. Finally, a 3-D CNN with dense connection modules extracts 3-D feature graphs from image patches and assigns each pixel to one of a few classes.

2.2 3-D Discrete Wavelet Transform

The three-dimensional discrete wavelet transform (3D DWT) is a mathematical tool for analysing three-dimensional data such as volumetric images or video sequences. It adds a dimension to the concept of the 2D discrete wavelet transform, allowing data to be decomposed along spatial, temporal, or spectral dimensions.

The 3D DWT works by breaking down a three-dimensional signal into multiple frequency sub bands and capturing both low and high-frequency components. This is accomplished using three stages of 1-D DWT. The first two stages of 3-D DWT are used to extract features from spatial content, and the final one is for the spectral dimension. In our experiment the down-sampling step is left out during 1-D DWT. So the size of the filtered cubes remains the same as original input cube.

The Haar wavelet is used as the fundamental wavelet in our strategy. We use a filter bank (L, H) comprising low-pass and high-pass filter coefficients, abbreviated as l[k] and h[k], respectively, to construct the 1-D discrete wavelet transform (DWT). We construct eight unique filtered hyperspectral cubes by convolving these filters with the hyperspectral cube along three dimensions. This procedure can be depicted as follows:

$X(h,w,b) = (L\ h \oplus H\ h) \otimes (L\ w \oplus H\ w) \otimes (L\ b \oplus H\ b)$

Where $\oplus$ denote space direct sum and $\otimes$ product.

After pre-processing with two-level 3-DWT on HIS cube, 15 filtered HIS cubes were obtained. Then, in the spectral dimension, the 15 hyperspectral cubes are concatenated. Finally, a new hyperspectral cube, denoted as $X \in R\ H \times W \times 15$ B, is obtained.

2.3 3-D Densely connected CNN

After extracting spatial and spectral information using 3-D DWT in the proposed approach in the next step, while maintaining the same spatial size, the PCA algorithm is applied to the wavelet cube across spectral bands. The spectral band count decreased from 15B to d. The most informative components are extracted using the PCA algorithm, which also substantially decreases the computational load on CNN. The labels of the small overlapped 3-D image patches created from the HSI cube are then determined by the central pixel of each patch. The extracted overlapped patches are used to subdivides into the training samples and the testing samples for the implemented network.

Figure 2 displays the proposed 3 D dense CNN framework for HSI classification. Our CNN architecture is based on 3-D CNN and includes dense connectivity. Our model's first three layers are 3-D convolutional layers; with 8 convolutional kernels

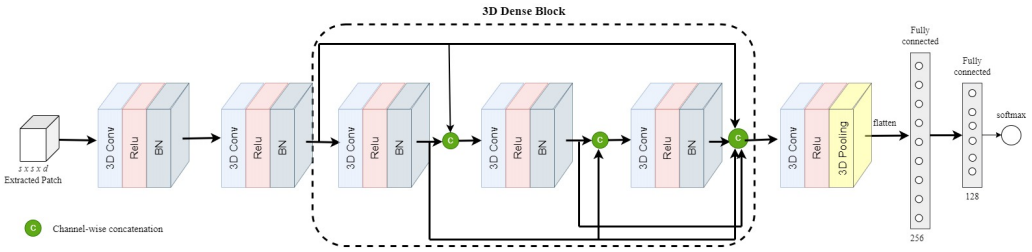

Fig 2. Flow chart of 3-D Dense CNN framework

of dimension 3 x 3 x 5 for al3-D input feature. Then, three 3-D convolutional layers with dense connection are added. Three-dimensional convolution layers with 16 filters are used throughout, and with the kernel size 3 x 3 x 3. Batch normalization is used after each 3D convolution to regularize the learning process and that also helps to avoid overfitting. The last convolution layer block with 16 filters and kernel size 1 x 1x 1 followed by 3-D pooling. Finally, 3D cubes are flattened to the classes. Finally, the 3-D feature cubes are flattened to 1-D, and the flattened layer is mapped to the number of classes using two fully connected layers. Dropout is employed in fully connected layers. The activation function was rectified linear units (ReLUs) after each convolution layer, and the optimizer 'Adam' is used to optimise the soft-max loss function after final fully connected layers are used.

Table 1. The layer wise summary of the implemented architecture with window size 9 x 9

Layer	Output Shape	Parameter
Input Layer	(9,9,15,1)	0
Conv3D_1 Batch Normalization_1	(7,7,9,8) (7,7,9,8)	512 32
Conv3D_2 Batch Normalization_2	(5,5,5,8) (5,5,5,8)	2888 32
Conv3D_3 Batch Normalization_3	(3,3,3,8) (3,3,3,8)	1736 32
Conv3D_4 Batch Normalization_4	(3,3,3,16) (3,3,3,16)	3472 64
Concatenation_1	(3,3,3,24)	0
Conv3D_5 Batch Normalization_5	(3,3,3,16) (3,3,3,16)	10384 64
Concatenation_2	(3,3,3,40)	0
Conv3D_6 Batch Normalization_6	(3,3,3,16) (3,3,3,16)	17296 64
Concatenation_3	(3,3,3,56)	0
Conv3D_7 Batch Normalization_7	(3,3,3,16) (3,3,3,16)	912 64
Flatten	16	0
Dense_1	256	4352
Dropout_1	256	0
Dense_2	128	32896
Dropout_2	128	0
Dence_3	7	903
Total Trainable Parameters=75,703		

The layer wise summary of the implemented architecture with window size 9 x 9 is shown in Table 1. The total number of parameters of the proposed model is 75,703.

2.4 Bloodstain detection dataset

Our experiments make use of hyperspectral images from the dataset described in (14) which is freely available to the public under an open license (the dataset can be assessed from https://zenodo.org/record/3984905). The dataset used in this paper has hyperspectral images of six different parts of one mock-up crime scene. The latter A-F are used to identify the different HSI frame as shown Figure 3.

Images in datasets are acquired using a SOC710 hyperspectral camera in a spectral range of 377–1046 nm with a total of 128 bands. As suggested by (Romaszewski et al., 2021)[14], we remove the noisy bands (0–4), (48–50) and (122–128), leaving 113

Fig 3. Illustration of the dataset, the mock-up of a forensic scene with locations of images A-F

bands.

Annotated hyperspectral images of blood and six other visually similar (artificial blood, tomato concentrate, ketchup, beetroot juice, poster, and acrylic paint) substances are included in the dataset. Images in the dataset were captured over several days to capture changes in spectra related to the time-related decay process of blood substances. Datasets images ware annotated hyperspectral pixels according to the visible substance, so each HSI can be treated as labelled examples.

Out of the six different images of the mock-up scene E, 'Comparison', is chosen for the experiment in this paper. Scene-E 'Comparison' RGB rendering image and its ground truth image are shown in Figure 3 (b) and Figure 3 (c) respectively. In scene-E, a trace of real blood and bloods look alike substances with eight different backgrounds is present. Scene-E 'Comparison' has wood, plastic, metal, and some red-hued fabric. These materials are arranged in vertical fashion, and blood and blood-like substances are placed horizontally on them. The image provides challenging and diverse environments for finding blood.

3 Results and Discussion

3.1 Experimental configuration

We use a hardware environment comprised of the Google Colab cloud platform and GPUs to evaluate the performance of our 3D DWTCNN architecture. We keep most of the environmental parameters constant when comparing different state-of-the-art methods. The entire dataset is divided into a 10%/90% split, with 5% used for training and 5% used for validation (i.e., 5% + 5% = 10%). The remaining 90% is considered a blind set (i.e., test set) for the final model evaluation.

As a feature extraction PCA is used in 2DCNN,3DCNN, Hybrid CNN, and 3D Dense models. In 3D DWT DENSE CNN model DWT is applied before PCA. The structure of DENSE and DWT DENSE keeps identical for comparison.

The Adam optimizer was given an optimum learning rate of 0.001 with a momentum of 0.9. As an activation function "relu" is used for all convolution layers except the last layer in each model. The last convolution layer used "softmax" is used. The HSI cube dimensions of 9 x 9, 11 X 11 and 13 x13 were used to maintain the validity of the results for different deep learning algorithms. The model has been trained for a total of 10 epochs.

3.2 Experimental Result

For comparing the performance of 3D DWT DENSE with a few training samples, we consider four state-of-the-art methods, including 2DCNN, 3DCNN, and Hybrid models. To evaluate the performance of above models, we use the overall accuracy (OA), average accuracy (AA), and Kappa coefficient, and we report the averaged results in Table 2 after ten independent runs in all experiments. Result shows that for HIS cube size of 9 x 9 3D DWT DENSE CNN model outperform all implemented methods. Where's for 11 x 11 and 13 x 13 HIS cube size along with the 3D DTW DENSE CNN model Hybrid CNN (3 layer of 3D CNN followed by a 2D CNN) also show good performance.

Table 2. Classification Accuracy Using 2DCNN, 3DCNN, Hybrid CNN, 3D Dense, and DWT-DENSE Performance

Methods	Window								
	9 x 9			11 x 11			13 x 13		
	OA	AA	kapp	OA	AA	kapp	OA	AA	kapp
2DCNN	83.44	78.40	81.55	83.02	78.10	82.01	84.03	93.80	83.67
3DCNN	93.68	91.96	92.96	93.95	88.45	91.93	90.35	86.71	89.26
Hybrid	96.05	95.04	95.54	96.12	**95.87**	**95..34**	**96.59**	96.20	96.01
DENSE	94.44	92.95	93.12	93.12	92.43	93.58	92.87	90.12	92.01
DWTDENSE	**97.07**	**97.24**	**97.41**	**96.67**	95.80	95.06	96.50	**96.41**	**96.23**

Table 3 shows Overall accuracy (OA), precision (P), recall (R), and F1score (F1) are computed during training the model to verify the performance of the proposed DWT DENSE CNN model when the mock-up scene E is used. It shows 97% overall accuracy. 3D DTW DENSE CNN model shows 99% precision for blood classification in mockup scenes.

Table 3. Blood Stain Classification Results using A Discrete Wavelet Transform and Dense CNN with window size 9 x 9

Sample	Precision	Recall	F1-Score
Blood	0.99	0.95	0.97
Ketchup	0.99	0.99	0.99
artificial blood	0.92	0.97	0.95
poster paint	1.00	1.00	1.00
tomato concentrate	0.98	0.90	0.94
acrylic paint	0.98	0.99	0.98
Accuracy			0.97
Macro avg.	0.98	0.97	0.97
Weighted avg	0.97	0.97	0.97

The performance of the proposed models has been evaluated using confusion matrices of the E scenario, as depicted in Figure 4. The 3D DWT DENSE CNN method achieves an average accuracy (AA) of 96.9% in classifying blood traces from other red hues, as depicted in Figure 3. In addition to the AA, the proposed method attains an overall accuracy (OA) of 97%.

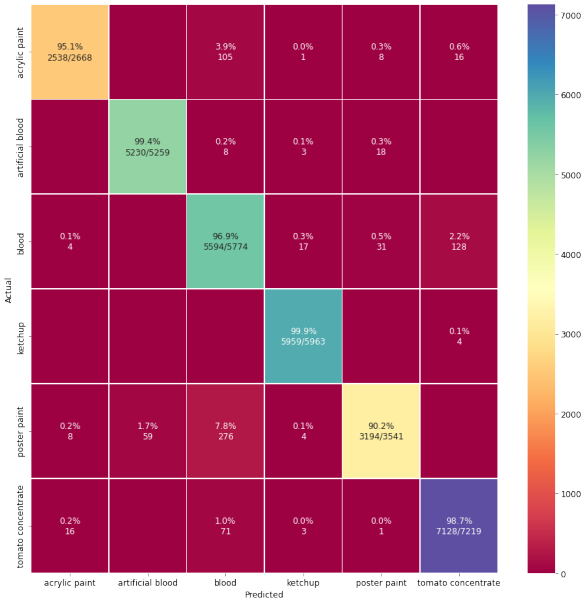

Fig 4. The confusion matrix using 3D DTW DENSE CNN Model

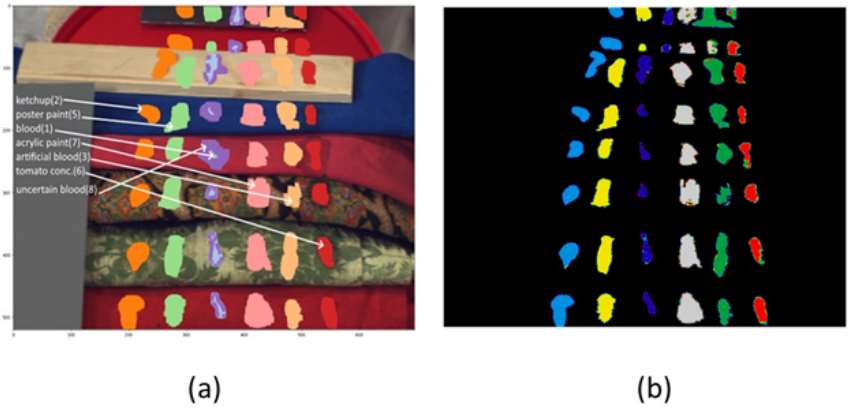

Fig 5. (a) Original Image frame "scene-E" with annotation (b) predicted Ground Truths using 3D DWT DWNSE CNN model

In addition, Figure 5 displays the classification accuracy for graphical maps (i.e., Ground Truths) attained by the 3D DWT DENSE CNN.

4 Conclusion

In this study, blood stains with various backgrounds and blood-like substance were detected using 2DCNN, 3DCNN, Hybrid CNN, Dense CNN, and 3D DWT DENSE CNN. The categorization performance of blood strain in mock crime senses was greatly enhanced by 3D DWT DENSE CNN, one of the several deep neural network models that had been applied. The total classification accuracy demonstrates the possible application of HIS to identify blood at complicated crime scenes without the need for a skilled lab technician or any destructive chemical techniques. The classification accuracy for the HSI using 3D DWT DENSE CNN is 97% overall.

A comparison of implemented models shows that the 3-D DWT can extract more discriminative features and that the dense connection module can be used to optimize the classification architecture of CNN. Combining dense 3-D CNN and 3-D DWT ensures classification performance, the network structure is made light and compact, and robust feature representation is possible. The experimental findings confirmed the advantages of our approach, which is particularly clear when the HSI has fewer training samples, a complicated background, and more visually comparable categories. As a future scope of the model can be tested with different images form same datasets utilizing transfer learning.

Future research should examine additional datasets for testing and evaluating our model, as well as applying transfer learning methods for HSI classification.

References

1) Sijen T, Harbison S. On the Identification of Body Fluids and Tissues: A Crucial Link in the Investigation and Solution of Crime. *Genes*. 2021;12(11):1–32. Available from: https://doi.org/10.3390/genes12111728.
2) Achetib N, Falkena K, Swayambhu M, Aalders MCG, van Dam A. Specific fluorescent signatures for body fluid identification using fluorescence spectroscopy. *Scientific Reports*. 2023;13(1):1–13. Available from: https://doi.org/10.1038/s41598-023-30241-7.
3) Khan MJ, Khan HS, Yousaf A, Khurshid K, Abbas A. Modern Trends in Hyperspectral Image Analysis: A Review. *IEEE Access*. 2018;6:14118–14129. Available from: https://ieeexplore.ieee.org/document/8314827.
4) Majda A, Wietecha-Posłuszny R, Mendys A, Wójtowicz A, zba Kopczyńska BŁ. Hyperspectral imaging and multivariate analysis in the dried blood spots investigations. *Applied Physics A*. 2018;124(4):1–8. Available from: https://doi.org/10.1007/s00339-018-1739-6.
5) Ahmad M, Shabbir S, Roy SK, Hong D, Wu X, Yao J, et al. Hyperspectral Image Classification—Traditional to Deep Models: A Survey for Future Prospects. *IEEE Journal of Selected Topics in Applied Earth Observations and Remote Sensing*. 2021;15:968–999. Available from: https://ieeexplore.ieee.org/document/9645266/authors.
6) Zulfiqar M, Ahmad M, Sohaib A, Mazzara M, Distefano S. Hyperspectral Imaging for Bloodstain Identification. *Sensors*. 2021;21(9):1–20. Available from: https://doi.org/10.3390/s21093045.
7) zek KK, Romaszewski M, Głomb P, Grabowski B, Cholewa M. Blood Stain Classification with Hyperspectral Imaging and Deep Neural Networks. *Sensors*. 2020;20(22):1–24. Available from: https://doi.org/10.3390/s20226666.
8) Butt MHF, Ayaz H, Ahmad M, Li JP, Kuleev R. A Fast and Compact Hybrid CNN for Hyperspectral Imaging-based Bloodstain Classification. In: 2022 IEEE Congress on Evolutionary Computation (CEC), 18-23 July 2022, Padua, Italy. IEEE. 2022;p. 1–8. Available from: https://ieeexplore.ieee.org/document/9870277.
9) Cao Z, Li X, Jianfeng J, Zhao L. 3D convolutional siamese network for few-shot hyperspectral classification. *Journal of Applied Remote Sensing*. 2020;14(04). Available from: https://doi.org/10.1117/1.JRS.14.048504.

10) Wang W, Dou S, Jiang Z, Sun L. A Fast Dense Spectral–Spatial Convolution Network Framework for Hyperspectral Images Classification. *Remote Sensing*. 2018;10(7):1–19. Available from: https://doi.org/10.3390/rs10071068.
11) Xu H, Yao W, Cheng L, Li B. Multiple Spectral Resolution 3D Convolutional Neural Network for Hyperspectral Image Classification. *Remote Sensing*. 2021;13(7):1–21. Available from: https://doi.org/10.3390/rs13071248.
12) Anand R, Veni S, Aravinth J. Robust Classification Technique for Hyperspectral Images Based on 3D-Discrete Wavelet Transform. *Remote Sensing*. 2021;13(7):1–19. Available from: https://doi.org/10.3390/rs13071255.
13) Xu J, Zhao J, Liu C. An Effective Hyperspectral Image Classification Approach Based on Discrete Wavelet Transform and Dense CNN. *IEEE Geoscience and Remote Sensing Letters*. 2022;19:1–5. Available from: https://ieeexplore.ieee.org/document/9792310.
14) Romaszewski M, Głomb P, Sochan A, Cholewa M. A dataset for evaluating blood detection in hyperspectral images. *Forensic Science International*. 2021;320:110701. Available from: https://doi.org/10.1016/j.forsciint.2021.110701.